

# Suzaku Spectroscopy Study of Hard X-Ray Emission in the Arches Cluster

Masahiro TSUJIMOTO

*Department of Physics, Rikkyo University, 3-34-1, Nishi-Ikebukuro, Toshima, Tokyo 171-8501.*

*tsujimot@ivs.rikkyo.ne.jp*

Yoshiaki HYODO and Katsuji KOYAMA

*Department of Physics, Graduate School of Science, Kyoto University,*

*Kita-shirakawa Oiwake-cho, Sakyo, Kyoto 606-8502.*

*hyodo@cr.scphys.kyoto-u.ac.jp, koyama@cr.scphys.kyoto-u.ac.jp*

(Received ; accepted )

## Abstract

We present the results of a Suzaku study of the Arches cluster in the Galactic center region. A high signal-to-noise ratio spectrum in the 3–12 keV band was obtained with the XIS (X-ray Imaging Spectrometer) onboard the Suzaku Observatory. We found that the spectrum consists of a thermal plasma, a hard power-law tail, and two Gaussian line components. The plasma component with a temperature of  $\sim 2.2$  keV is established from the presence of Ca XIX and Fe XXV  $K\alpha$  lines as well as the absence of Fe XXVI  $K\alpha$  line. The two Gaussian lines represent the  $K\alpha$  and  $K\beta$  lines from iron at lower ionization stages at  $\sim 6.4$  and  $\sim 7.1$  keV. Both the line centers and the intensity ratio of these two lines are consistent with the neutral iron. The hard power-law tail with a photon index of  $\sim 0.7$  was found to have no pronounced iron K edge feature. In comparison with the published Chandra spectra constructed separately for point-like and diffuse emission, we conclude that the thermal component is from the ensemble of point-like sources plus thermal diffuse emission concentrated at the cluster center, while the Gaussian and the hard tail components are from the non-thermal diffuse emission extended in a larger scale. In the band-limited images of the XIS field, the distribution of the 7.5–10.0 keV emission resembles that of the 6.4 keV emission, including the local excess at the Arches cluster. This strongly suggests that the power-law emission is related to the 6.4 and 7.1 keV lines in the underlying physics. We discuss two ideas to explain both the hard continuum and the lines: (1) X-ray photoionization that produces fluorescence lines and the Thomson scattering continuum and (2) non-thermal electron impact ionization of iron atoms and bremsstrahlung continuum. But whichever scenario is adopted, the photon or particle flux from the Arches cluster is too low to account for the observed line and continuum intensity.

**Key words:** X-rays: ISM — Galaxy: center — Galaxy: open clusters: individual (Arches Cluster)

## 1. Introduction

The central  $\sim 200$  pc of the center of our Galaxy is particularly rich in curious spatial and spectral features. One of the features distinctively seen in the Galactic center region is the diffuse iron  $K\alpha$  line emission at  $\sim 6.4$  keV (Koyama et al. 1996). The line originates from neutral or low-ionized iron (hereafter quoted as FeI), but its ionizing mechanism is not yet understood. Two major ideas have been developed. One is fluorescence from photo-ionized iron (Sunyaev et al. 1993; Koyama et al. 1996; Revnivtsev et al. 2004). The X-ray spectrum from the Sagittarius B2 cloud, which is characterized by the strong  $\sim 6.4$  keV emission line and the  $\sim 7.1$  keV iron K edge, is best accountable by this model (Koyama et al. 1996; Murakami et al. 2000). Another idea is that iron is ionized by accelerated electrons (Yusef-Zadeh et al. 2002b; Predehl et al. 2003; Wang et al. 2006).

The distribution of the diffuse 6.4 keV emission is highly asymmetric around the Galactic center with a bias in the north-east direction (Koyama et al. 1996; Koyama et al.

2006b) and appears filamentary (Park et al. 2004). Of particular interest is the 6.4 keV emission associated with the Arches cluster, which is one of the richest and the most densely packed massive star clusters in our Galaxy.

The cluster has a total mass of  $\sim 10^4 M_{\odot}$ , a compact size with a diameter of  $\sim 15''$  ( $\sim 0.6$  pc at an assumed distance of 8.5 kpc), a stellar mass density of  $\sim 3 \times 10^5 M_{\odot} \text{ pc}^{-3}$ , and an estimated age of 2–4.5 Myr (Nagata et al. 1995; Cotera et al. 1996; Serabyn et al. 1998; Figer et al. 1999; Blum et al. 2001; Yang et al. 2002; Stolte et al. 2002; Figer et al. 2002; Figer 2005). It contains  $\sim 5\%$  of all the known Wolf-Rayet stars in our Galaxy (Figer 2005), which are characterized by a large mass loss rate reaching  $\sim 10^{-4} M_{\odot} \text{ yr}^{-1}$  (Lang et al. 2001; Lang et al. 2005). The level of high mass star-forming activity of the Arches cluster, which can be measured by the number of O stars, is comparable only to NGC 3603 (Moffat 1983), W49A (Conti & Blum 2002; Alves & Homeier 2003), and Westerlund 1 (Clark et al. 2005) in our Galaxy and R136 at the center of 30 Doradus (Campbell et al. 1992) in the Large Magellanic

Cloud.

Yusef-Zadeh et al. (2002a) first reported the detection of two point sources in addition to diffuse emission from this region using the Chandra X-ray Observatory (Weisskopf et al. 2002). The extended X-ray emission is elongated beyond the cluster boundary with a size of  $\sim 60'' \times 90''$  and its spectrum can be fit with a thermal model with a temperature of  $\sim 5.7$  keV in addition to a  $\sim 6.4$  keV line (Yusef-Zadeh et al. 2002a). Based on these claims, the hard diffuse emission is considered an example of the cluster wind plasma, which is a collection of interacting stellar winds from massive stars in a cluster (Cantó et al. 2000; Raga et al. 2001; Silich et al. 2004; Rockefeller et al. 2005). However, the poor spectrum of the extended emission does not allow a conclusion to be drawn about a thermal origin. Law & Yusef-Zadeh (2004) cautioned that the continuum emission can also be fit by a power-law, and can thus be explained by non-thermal emission. Recent results based on a longer exposure Chandra observation by Wang et al. (2006) indicated that the cluster wind is only seen at the cluster center, and the majority of the diffuse emission is composed of a strong 6.4 keV line and a power-law continuum emission of non-thermal origin.

In order to understand the nature of the X-ray emission in the Arches cluster and the diffuse 6.4 keV emission ubiquitous in, but exclusive to, the Galactic center region, hard-band X-ray spectroscopy with high signal-to-noise ratio (S/N) is obviously a key. The bandpass includes both thermal (Fe XXV  $K\alpha$  and Fe XXVI  $K\alpha$  at  $\sim 6.7$  and  $\sim 7.0$  keV) and fluorescent (Fe I  $K\alpha$  and  $K\beta$  at  $\sim 6.40$  and  $\sim 7.05$  keV) features as well as the iron K absorption edge feature at  $\sim 7.11$  keV. The underlying power-law continuum, if it ever exists, is visible at energies  $\gtrsim 8$  keV, where the thermal contribution plays a minor role. Moreover, the hard X-rays penetrate through the large attenuation of  $A_V \sim 30$  mag common toward the Galactic center region (Morris & Serabyn 1996).

Here, we present the results of a spectroscopic study of the hard emission in the Arches cluster using the Suzaku Observatory. The XIS (X-ray Imaging Spectrometer; Koyama et al. 2006a) onboard Suzaku (Mitsuda et al. 2006) provides high S/N spectra in the hard-band aided by the excellent spectroscopic performance of the CCDs and the large effective area of the X-ray optics. To complement the moderate spatial resolution of Suzaku, we refer to the recent Chandra results by Wang et al. (2006) and results obtained by our own reduction of the same dataset.

## 2. Observations and Data Reduction

Two observations of the Galactic center region were conducted using Suzaku during the performance verification phase on 2006 September 23 and 30. Suzaku observations provide simultaneous XIS and HXD (Hard X-ray Detector; Takahashi et al. 2006; Kokubun et al. 2006) data. We concentrate on the XIS data with a combined integration time of  $\sim 95$  ks. The XIS field is centered at (R. A., Decl.) = ( $17^{\text{h}}46^{\text{m}}03^{\text{s}}$ ,  $-28^{\circ}55'32''$ ) in the equinox

J2000.0. The off-axis angle of the Arches cluster is  $\sim 6'.6$ .

The XIS is equipped with four X-ray CCDs. Three of them (XIS0, 2, and 3) are front-illuminated (FI) CCDs and the remaining one (XIS1) is a back-illuminated (BI) CCD that is superior in the soft band responses. They are mounted at the focus of four independent X-ray telescopes (XRT; Serlemitsos et al. 2006). The detectors are sensitive in the energy range of 0.2–12.0 keV with an initial energy resolution of  $\sim 130$  eV in the full width half maximum<sup>1</sup> at 5.9 keV ( $R \sim 45$ ) and a total effective area of  $\sim 590$  cm<sup>2</sup> at 8 keV. An XIS field of view covers a  $\sim 18' \times 18'$  region with a half power diameter (HPD) of  $\sim 1'.9$ . The HPD is almost independent of the off-axis angle within  $\sim 10\%$  (Shibata et al. 2001).

Data were taken by the XIS normal mode and screened to remove events during the South Atlantic Anomaly passages and earth elevation angles below 5 degrees. There are standard radioactive sources of <sup>55</sup>Fe installed in two corners of each of the four CCDs. These calibration sources were used to determine the absolute gain. In addition, we can utilize the observed intense emission lines from the hot gas filling the Galactic center region (Koyama et al. 2006b). Assuming that the center energy of Fe and S  $K\alpha$  lines in the diffuse spectrum is spatially uniform, we corrected for the charge transfer inefficiency and fine-tuned the energy gain across the chips. These calibration processes were performed using the same dataset with the presented analysis. Resultantly, the systematic energy uncertainty of XIS is as low as  $\sim +3/-6$  eV at 6 keV. The details of the calibration of the Galactic center datasets are described in Koyama et al. (2006b).

## 3. Analysis

### 3.1. Image

Figure 1 shows the band-limited XIS images in the (a) 6.25–6.55, (b) 6.55–6.85, and (c) 7.5–10.0 keV bands. The former two bands contain  $K\alpha$  emission lines from iron at low and high ionization stages, respectively. The 7.5–10.0 keV image complements the one below 8.0 keV by Chandra; the effective area at 8 keV of Suzaku XIS is larger than that of Chandra ACIS (Advanced CCD Imaging Spectrometer; Garmire et al. 2003) by more than ten-fold. A significant excess is seen at the position of the Arches cluster in all bands, which is elevated from the diffuse emission at the north east of the Galactic center. Due to the limited spatial capability of Suzaku XIS, it is difficult to discriminate point sources from the underlying diffuse emission in the Arches cluster.

The 7.5–10.0 keV image (Fig. 1c) morphologically resembles the 6.4 keV image (Fig. 1a) more than the 6.7 keV image (Fig. 1b). In particular, both the 7.5–10.0 keV and the 6.4 keV images have a local excess centered at the radio arc bubble located at about  $(l, b) = (0.13^\circ, -0.11^\circ)$ . The correlation between the 6.4 keV emission and the ra-

<sup>1</sup> The spectral resolution keeps degrading in the orbit. We included a degradation of  $\sim 30$  eV ( $1 \sigma$ ) for the presented analysis, which was measured from the same dataset (Koyama et al. 2006b).

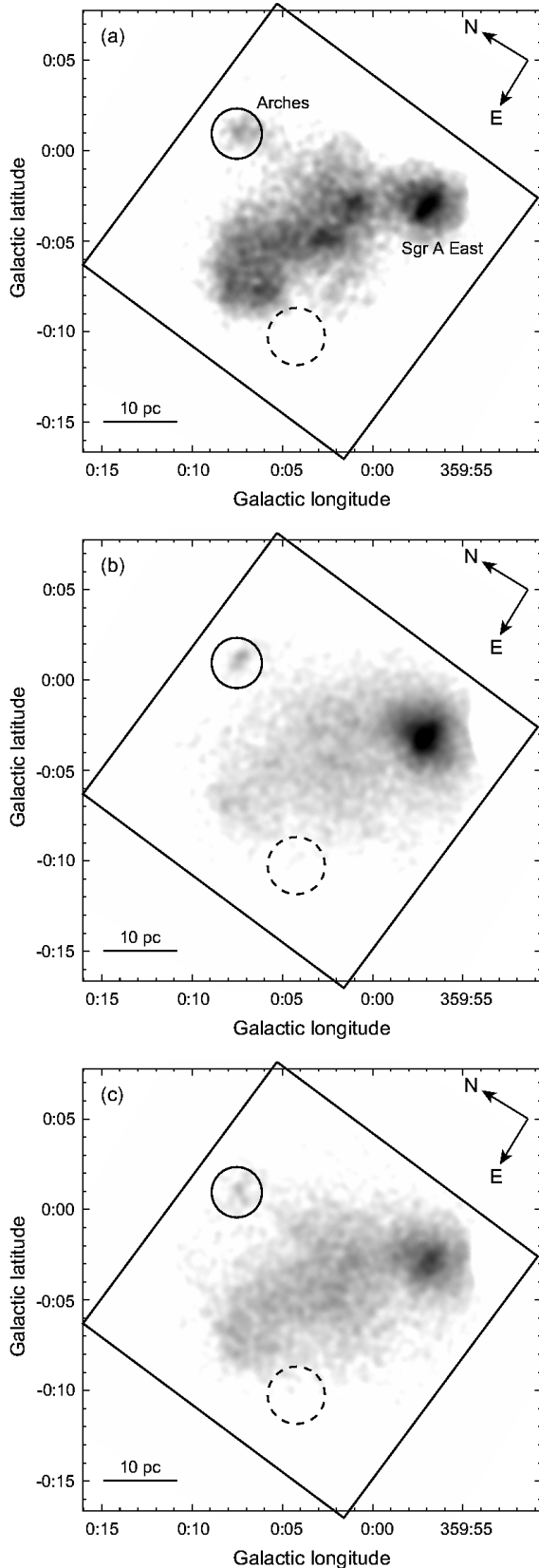


**Fig. 1.** Band-limited smoothed X-ray images by XIS: (a) 6.25–6.55, (b) 6.55–6.85, and (c) 7.5–10.0 keV ranges. The data from the four CCDs are merged. Solid and dotted circles show the source and background accumulation regions, respectively. The four corners of the images are masked out to remove signals from calibration sources.

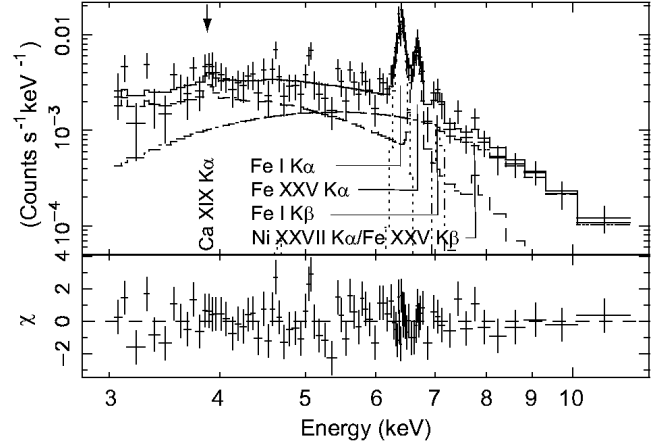


**Fig. 2.** XIS spectrum of the Arches cluster composed of point-like and diffuse emission. Grouped and background-subtracted data with uncertainties are plotted in the upper panel. The best-fit model convolved with the mirror and detector responses are shown by the broken (each component) and solid (total) lines. The lower panel shows the residuals of the fit.

dio arc bubble was found by Rodríguez-Fernández et al. (2001). Also, the 6.7 keV image has the dominating peak at the Sagittarius A East, while the 6.4 keV and 7.5–10.0 keV images have extended emission across the field with a similar surface brightness.

### 3.2. Spectrum

Figure 2 shows the background-subtracted XIS spectrum of the Arches cluster constructed from the three FI chip data. The source spectrum was extracted from a circle around the local intensity peak of a smoothed XIS image (solid circle in Fig. 1), while the background was accumulated from a position devoid of intense diffuse emission and at a similar off-axis angle (dashed circle in Fig. 1). We tried several different positions for the background subtraction and found that the spectrum above  $\sim 3$  keV is insensitive to the background positions. The spectrum below  $\sim 3$  keV is contaminated by the inhomogeneous diffuse emission typical to the Galactic center region, hence is not used hereafter. A radius of  $1/6$ , which is the  $\sim 80\%$  encircled energy radius of a point source, is used for the background extraction circle. A smaller radius of  $1/4$  is used for the source circle to maximize the S/N.

The spectrum is characterized by a complex of iron lines in the 6.0–8.0 keV band over a hard continuum. The three most conspicuous lines are attributable to the  $K\alpha$  line from highly ionized iron (Fe XXV) at  $\sim 6.7$  keV, and  $K\alpha$  and  $K\beta$  lines from neutral or low-ionized iron (Fe I) at  $\sim 6.4$  and  $\sim 7.1$  keV, respectively. The existence of Fe XXV  $K\alpha$  in addition to Ca XIX  $K\alpha$  ( $\sim 3.9$  keV) and Ni XXVII  $K\alpha$  + Fe XXV  $K\beta$  (7.8–7.9 keV) lines indicates a thermal plasma with a temperature of a few keV, while Fe I K lines and a hard continuum up to  $\sim 12$  keV suggest additional components.

We first fitted the spectrum with photo-electrically absorbed thin-thermal plasma (APEC; Smith et al. 2001)

model to determine the plasma temperature ( $k_{\text{B}}T$ ) and the amount of interstellar extinction ( $N_{\text{H}}$ ). The abundance relative to solar was derived separately for elements with prominent emission lines. Two Gaussian components were added to the model to account for the lines at  $\sim 6.4$  and  $\sim 7.1$  keV. Their line center ( $E_1$  and  $E_2$ ) and photon flux ( $N_1$  and  $N_2$ ) were also determined by the fit. The widths of the lines were consistent with zero.

The resultant best-fit model was marginally acceptable with the null hypothesis probability of the  $\chi^2$  value ( $P_{\chi^2}$ ) of 0.01. A significant residual above  $\sim 7$  keV obviously requires an additional component. We added a power-law component to reach an acceptable fit. An additional thermal component also yielded an acceptable fit, but the best-fit temperature of  $>20$  keV is unphysical. We therefore continued with the power-law component.

The final fit result ( $P_{\chi^2}=0.28$ ) is summarized in Table 1. Here, we fixed the abundance to be solar for all the elements upon the confirmation that the best-fit value is consistent with solar. Also,  $E_2$  and  $N_2$  are tied to  $E_1$  and  $N_1$  respectively, as the best-fit values are consistent with the ones expected for the neutral iron  $\text{K}\alpha$  and  $\text{K}\beta$  lines. By separating the Fe I  $\text{K}\beta$  line at  $\sim 7.05$  keV, the Fe XXVI  $\text{K}\alpha$  line at  $\sim 6.97$  keV and the Fe K edge at  $\sim 7.11$  keV are found to be absent. The absence of the Fe XXVI line as well as the existence of the Fe XXV line contributes for a tight constraint of the plasma temperature. The  $N_{\text{H}}$  is common for all the components. The X-ray flux and luminosity ( $F_{\text{X}}$  and  $L_{\text{X}}$ ) in the 3.0–10.0 keV band were calculated separately for the thermal and the power-law components. The  $L_{\text{X}}$  value is corrected for the absorption with the distance to the source assumed to be 8.5 kpc.

## 4. Discussion

### 4.1. Origin of Three Spectral Components

We identified three spectral components (thermal, power-law, and two Gaussian lines) in the XIS spectrum. Wang et al. (2006) conducted spatially-resolved Chandra spectroscopy of the Arches cluster in the 2–8 keV band and revealed a more detailed spatial structure upon the results by Yusef-Zadeh et al. (2002a); Law & Yusef-Zadeh (2004). The Arches X-rays consist of three spatial components: (1) point-like sources with a thermal spectrum, (2) diffuse emission with a thermal spectrum in a  $\sim 30''$  scale, and (3) diffuse emission with a  $\sim 6.4$  keV line over a power-law continuum in a more extended scale ( $\sim 60'' \times 90''$  by Yusef-Zadeh et al. 2002a). The former two thermal components are concentrated at the cluster center, in which three brightest point sources dominates the total emission. The last non-thermal component extends toward the southeast direction of the cluster. We consider that the thermal component in the XIS spectrum is from the ensemble of point sources plus the thermal diffuse emission at the cluster center, while the  $\sim 6.4$  keV and the accompanying  $\sim 7.1$  keV lines as well as the power-law continuum are from the larger diffuse emission.

In order to compare directly the best-fit spectral model parameters between the ACIS and XIS spectra, we re-

duced the Chandra ACIS data and obtained the best-fit parameters for the composite of the three brightest point sources and the extended emission. The parameters from XIS and ACIS spectral analysis agree with each other with overlapping 90% confidence ranges. For the thermal component, the XIS spectrum has a temperature of 2.2 (1.6–3.8) keV and the APEC normalization of  $3.2 (1.2\text{--}7.8) \times 10^{-3} \text{ s}^{-1} \text{ cm}^{-2} \text{ keV}^{-1}$ , while the ACIS spectrum has 2.0 (1.9–4.4) keV and  $2.5 (1.8\text{--}3.0) \times 10^{-3} \text{ s}^{-1} \text{ cm}^{-2} \text{ keV}^{-1}$ . For the power-law component, the photon index in the XIS spectrum is 0.72 (0.0–1.4), while that in the ACIS diffuse spectrum is 1.2 (0.80–1.8). For the Gaussian lines, the photon flux of the  $\sim 6.4$  keV line is  $2.1 (1.8\text{--}2.5) \times 10^{-5} \text{ s}^{-1} \text{ cm}^{-2}$  in XIS and  $2.3 (2.0\text{--}2.9) \times 10^{-5} \text{ s}^{-1} \text{ cm}^{-2}$  in ACIS. The equivalent width of the line against the power-law component is  $\sim 1.42$  keV in XIS and  $\sim 1.25$  keV in ACIS, indicating that the power-law flux as well as the line flux is consistent between the two.

### 4.2. Diffuse Medium

The high S/N spectra obtained with the XIS give a stringent constraint on the center energy of the  $\sim 6.4$  keV line, which is an increasing function of the ionization stage of iron. The fluorescent line energy is also affected by whether and how the atom is bound in molecules, but the resultant shifts are negligible of  $\sim 1$  eV (Paerels 1998). The best-fit value is consistent with the  $\text{K}\alpha$  line from neutral iron (6.40 keV). This is in agreement with the general understanding that most of iron in the ISM is in the form of dust (Sofia et al. 1994). However, slightly low ionization stages are also allowed up to about fourteenth (Fe XV; House 1969), including the systematic uncertainty of the XIS energy gain of  $\sim +3/-6$  eV.

### 4.3. Cause of Line and Power-law Emission

From the XIS spectrum (Fig. 2), we found that the power-law component extends up to  $\sim 12$  keV and dominates the spectrum above  $\sim 8$  keV. From the band-limited XIS images (Fig. 1), we noticed a similarity in the spatial distribution between the 7.5–10.0 keV and the 6.4 keV emission. This indicates that the power-law emission is related to the 6.4 keV line in the underlying physical process. Therefore, the power-law component and the Fe I lines need to be explained simultaneously. The equivalent width of the lines and the normalization of the power-law comprise two major observational tests to discriminate ideas on the origin of the emission. We examine two mechanisms (photoelectric ionization and electron impact ionization) and derive the conditions for the primary ionizing beam. In the former, the Thomson scattering continuum and the fluorescence are respectively responsible for the power-law and the line emission. In the latter, non-thermal electron bremsstrahlung and the K shell vacancy filling after the electron ionization are considered.

#### 4.3.1. Photoelectric Ionization

We first note that the lack of a prominent absorption edge feature at  $\sim 7.11$  keV alone does not constitute evidence against photoionization (Revnivtsev et al. 2004). This is expected when the reflecting matter is optically-



Table 1. XIS Spectroscopy.

Components	Par.	Units	Values*
Extinction	$N_{\text{H}}$	$\text{cm}^{-2}$	$14 (9.1\text{--}19) \times 10^{22}$
Thermal	$k_{\text{B}}T$	keV	2.2 (1.6–3.8)
	$F_{\text{X}}^{\dagger}$	$\text{erg s}^{-1} \text{cm}^{-2}$	$5.2 (2.0\text{--}13) \times 10^{-13}$
Power-law	$L_{\text{X}}^{\dagger}$	$\text{erg s}^{-1}$	$8.8 (3.4\text{--}21) \times 10^{33}$
	$\Gamma$		0.72 (0.0–1.4)
	$F_{\text{X}}^{\dagger}$	$\text{erg s}^{-1} \text{cm}^{-2}$	$7.3 (1.6\text{--}28) \times 10^{-13}$
Gaussian	$L_{\text{X}}^{\dagger}$	$\text{erg s}^{-1}$	$9.3 (2.0\text{--}36) \times 10^{33}$
	$E_1$	keV	6.41 (6.40–6.42)
	$N_1$	$\text{s}^{-1} \text{cm}^{-2}$	$2.1 (1.8\text{--}2.5) \times 10^{-5}$
	$E_2$	keV	$7.07 = 1.103 \times E_1$
	$N_2$	$\text{s}^{-1} \text{cm}^{-2}$	$2.4 \times 10^{-6} = 0.113 \times N_1$

\* Uncertainties in the parentheses indicate the 90% confidence range.

† Values in the 3.0–10.0 keV band.

thin to the primary radiation. In fact, the optically-thin approximation is justified by the Chandra result on the Arches cluster, wherein the power-law emission suffers an extinction accountable only by the ISM extinction to the Galactic center region ( $\sim 6 \times 10^{22} \text{ cm}^{-2}$ ; Wang et al. 2006).

We assume that the observed continuum emission does not include the direct X-rays. If it does, the equivalent width of the iron  $K\alpha$  fluorescent line is expected to be  $\lesssim 180 \text{ eV}$  (Reynolds & Nowak 2003; Tsujimoto et al. 2005) for the solar abundance, which contradicts the observed value. The equivalent width of the fluorescent line against the Thomson scattering continuum is expressed as a function of the ratio between the photoelectric and Thomson scattering cross sections, the ratio of the target (electron and iron atom) densities, and the geometry; the Thomson scattering is angle-dependent while the fluorescence is spherically symmetric (Liedahl 1998). Assuming that the incident X-ray spectrum is  $I(E)$ , the electron and iron densities of the reflecting medium are uniform ( $n_e$  and  $n_{\text{Fe}}$ , respectively), the photoelectric absorption cross section by iron is  $\sigma_{\text{P}}^{\text{Fe}}(E)$ , the differential Thomson scattering cross section is  $(d\sigma_{\text{T}}/d\Omega)(\theta)$  where  $\theta$  is the angle between the incident and scattered X-rays, the  $K\alpha$  fluorescence yield is  $Y_{K\alpha}$ , and the K edge energy is  $\chi$ , the equivalent width of the  $K\alpha$  line is given by

$$\text{EW}_{K\alpha} = Y_{K\alpha} \left( \frac{n_{\text{Fe}}}{n_e} \right) \left( 4\pi \frac{d\sigma_{\text{T}}}{d\Omega}(\theta) \right)^{-1} \times \left( \frac{\int_{\chi}^{\infty} dEI(E)\sigma_{\text{P}}^{\text{Fe}}(E)}{I(E=6.4 \text{ keV})} \right). \quad (1)$$

By substituting  $Y_{K\alpha} \sim 0.34$  (Kortright 2001),  $n_{\text{Fe}}/n_e \sim n_{\text{Fe}}/n_{\text{H}} \sim 3 \times 10^{-5}$  (Däppen 2000) where  $n_{\text{H}}$  is the hydrogen density,  $d\sigma_{\text{T}}/d\Omega(\theta) \sim 4.0 \times 10^{-26} (1 + \cos^2\theta) \text{ cm}^2$ ,  $I(E) \propto E^{-\Gamma}$ , and  $\sigma_{\text{P}}^{\text{Fe}}(E) = 2 \times 10^{-20} (E/7.1 \text{ keV})^{-3} \text{ cm}^2$  (Gullikson 2001), we obtain

$$\text{EW}_{K\alpha} \sim 3 \left( \frac{1}{\Gamma + 2} \right) \left( \frac{6.4}{7.1} \right)^{\Gamma} \left( \frac{1}{1 + \cos^2\theta} \right) \text{ keV}. \quad (2)$$

We can determine both  $\text{EW}_{K\alpha}$  and  $\Gamma$  observationally, resulting in  $\theta \approx 50$  degrees using the best-fit values.

In practice, though, higher accuracy in the parameter determination is required for a meaningful geometrical constraint. The observed  $\text{EW}_{K\alpha}$  is easily explained by the photoionization interpretation. For the amplitude of continuum emission, the incident flux of  $I(E) \sim 3 \times 10^7 (n_e/10^2 \text{ cm}^{-3})^{-1} \text{ s}^{-1} \text{ cm}^{-2} \text{ keV}^{-1}$  is required at 10 keV. Here, the diffuse medium is assumed to have a spherical shape of a 3 pc diameter. The estimate of the electron density is from Rodríguez-Fernández et al. (2001).

To summarize, the photoionization interpretation requires the following conditions: (1) the primary source is an external source, (2) the incident spectrum has a power of  $\Gamma \sim 1$  and (3) a photon flux of  $\sim 10^7 \text{ s}^{-1} \text{ cm}^{-2} \text{ keV}^{-1}$  at 10 keV, (4) the direct emission is optically thin to the reflecting medium (i.e.,  $n_{\text{H}} < 2 \times 10^5 \text{ cm}^{-2}$ ), and (5) the reflecting geometry should satisfy the constraint on  $\theta$ .

No source is found for the primary source in the vicinity at present. The point sources in the Arches cluster can be excluded. This is simply because the continuum emission by the Thomson scattering cannot exceed the illuminating thermal emission above the iron K edge energy, which is contrary to the XIS spectrum showing stronger non-thermal emission than thermal emission at the band (Fig. 2). Wang et al. (2006) also discussed that Arches point sources are too dim for the fluorescent lines.

#### 4.3.2. Electron Ionization

Another favored interpretation for the cause of the  $\sim 6.4 \text{ keV}$  line is the vacancy filling after the iron K shell ionization by low energy electrons with an energy of 10–100 keV. This was proposed to explain the Galactic ridge diffuse X-ray emission (Valinia et al. 2000), in which they claimed that the low energy electrons with a density of  $\sim 0.2 \text{ eV cm}^{-3}$  and the power-law spectrum of an index of  $\sim 0.3$  contribute significantly to both the observed line and continuum emission. Yusef-Zadeh et al. (2002b) and Wang et al. (2006) employed this model to account for the  $\sim 6.4 \text{ keV}$  line observed in G0.13–0.13 and the Arches cluster in the Galactic center region, respectively.

The calculation of expected line and continuum intensity of this process requires numerical treatments because of the complex dependence of the cross sections on the

electron and X-ray energy. A detailed computation is given in Tatischeff (2002). Two important things have to be considered. First, the electron beam is stopped at the surface of the hydrogen column. The stopping range for 10 and 100 keV electrons is  $\sim 7 \times 10^{19} m_H$  and  $\sim 4 \times 10^{21} m_H \text{ g cm}^{-2}$  where  $m_H$  is the hydrogen mass (Tatischeff 2002). Second, the energy conversion rate from the electron beam to the X-ray bremsstrahlung is quite small with an order of  $\sim 10^{-5}$ .

With these kept in mind, we can compare the expected and observed values. The equivalent width of the iron  $K\alpha$  line against the Bremsstrahlung continuum is expected to be  $\sim 290 \text{ eV}$  (Tatischeff 2002), which is smaller than the observed value. An iron abundance of 4–5 times larger than the solar value needs to be introduced to reconcile the discrepancy, though no such indication is present for the Arches cluster. From the spectral fit of the XIS spectrum, we found that a solar abundance for iron accounts for the observed Fe XXV  $K\alpha$  line intensity over the continuum. Wang et al. (2006) suggested that the iron abundance is  $\sim 2$  from the X-ray spectral fits of point sources in the cluster. Najjarro et al. (2004) conducted near-infrared spectroscopy of the photospheric emission of Wolf-Rayet stars in the Arches cluster and found that the abundance is consistent with solar.

For the level of continuum emission, we can consult Figure 7 in Tatischeff (2002), which illustrates the X-ray production rate by the low energy electron impact. The injected electrons are assumed to have a total energy rate of  $1 \text{ erg s}^{-1}$  in an energy range of 10–100 keV and the power-law number density with an index of 2. At 10 keV, a continuum photon production rate of  $\sim 8 \times 10 \text{ s}^{-1} \text{ keV}^{-1}$  is expected. We observed  $\sim 1.1 \times 10^{-5} \text{ s}^{-1} \text{ cm}^{-2} \text{ keV}^{-1}$  at 10 keV in the XIS spectrum, which can be converted to  $\sim 9.5 \times 10^{40} \text{ s}^{-1} \text{ keV}^{-1}$  at a distance of 8.5 kpc. Therefore, an electron injection rate of  $\sim 1 \times 10^{39} \text{ erg s}^{-1}$  is required. Assuming that the diffuse medium is “optically-thick” to the electron beam, we can derive the required flux of the injected electrons to be  $\sim 2 \times 10^1 \text{ erg s}^{-1} \text{ cm}^{-2}$  regardless of the target density. Integrating over the entire mass of the medium (Yusef-Zadeh et al. 2002b; Wang et al. 2006) may lead to a significant overestimation.

To summarize, the electron ionization interpretation requires the following conditions: (1) the electron beam has an incident flux of  $\sim 2 \times 10^1 \text{ erg s}^{-1} \text{ cm}^{-2}$  and (2) an index of  $\sim 2$  for the injected power-law number density, and (3) 4–5 times larger abundance than solar for iron in the diffuse medium.

We do not have a list of electron accelerators with an estimated energy injection rate in the Galactic center region and further studies must be undertaken to elucidate the primary source. However, we can at least claim that the accelerated electrons by wind-wind collisions in the Arches cluster (Wang et al. 2006) are unlikely the case. This is simply because the total kinetic energy rate via stellar winds is smaller by an order than the required electron energy injection rate. Here the total energy rate is calculated from an assumed wind velocity of  $\sim 1000 \text{ km s}^{-1}$  and a mass loss rate of  $\sim 10^{-4} M_\odot \text{ yr}^{-1}$  estimated by the

free-free emission intensity at the centimeter continuum (Lang et al. 2005).

Protons accelerated via wind-wind collisions to have an MeV energy may cause both the bremsstrahlung and the iron line emission in a similar manner as electrons with several tens of keV. However, because the bremsstrahlung conversion rate for protons is as inefficient as that of electrons (Uchiyama et al. 2002), the protons ionization will encounter the same energy budget deficit.

Finally, heavy ions with an MeV  $\text{amu}^{-1}$  energy are also capable of producing the continuum emission by inverse bremsstrahlung and the iron line emission by K shell ionization. In this case, however, the resultant lines are broader and bluer than the case of proton or electron ionization by  $\sim 50 \text{ eV}$  (e.g., Burch et al. 1971), which disagrees with the iron  $K\alpha$  line center determined from the XIS spectrum. Therefore, the ionization by heavy ions can be excluded regardless of whether they are accelerated by wind-wind collisions in the Arches cluster or somewhere else in the Galactic center region.

## 5. Summary

We conducted a spectroscopy study of the hard X-ray emission in the Arches cluster using the Suzaku XIS data during the performance verification phase. We obtained a high signal-to-noise spectrum in the 3.0–12 keV range, which consists of a thermal ( $k_B T \sim 2.2 \text{ keV}$ ), a power-law ( $\Gamma \sim 0.7$ ), and two Gaussian line ( $E \sim 6.4$  and  $\sim 7.1 \text{ keV}$ ) components. The thermal emission is from an ensemble of point sources plus compact thermal diffuse emission at the center of the Arches cluster, while the power-law and the Gaussian components are from the more extended diffuse medium associated with the cluster. The  $\sim 6.4$  and  $\sim 7.1 \text{ keV}$  emission lines are considered to be  $K\alpha$  and  $K\beta$  lines from neutral iron.

From the band-limited images, we found a similarity in the spatial distribution between the 6.4 keV and 7.5–10.0 keV emission across the XIS field, including the local excess at the Arches cluster. This strongly suggests that the power-law emission is related to the 6.4 and 7.1 keV line emission in its origin.

Two ideas are examined to account for both the continuum and line emission; the photoelectric ionization in which the Thomson scattering and the fluorescence are respectively responsible for the continuum and the line emission, and the electron impact ionization in which the bremsstrahlung and the K shell vacancy filling are respectively for the continuum and the lines. Whichever the case, the Arches cluster is unlikely the primary source.

We have shown that the combined measurements of both the line and the continuum emission give a tight constraint on the primary source. There are dozens of  $\sim 6.4 \text{ keV}$  clumps in the Galactic center region, and the present results in the Arches cluster illustrate that Suzaku XIS spectroscopy is a powerful tool for characterizing the  $K\alpha$  and  $K\beta$  lines as well as the underlying power-law emission. Another report of a  $\sim 6.4 \text{ keV}$  emitter can be found in this volume (Koyama et al. 2006c). All these new pieces

of evidence on both types of emission should eventually be combined to reach a unified picture of this curious phenomenon.

The authors express gratitude to the diligent work by the Suzaku team and the helpful comments on the draft by Richard L. Kelly. M. T. acknowledges the hospitality at the Department of Physics, Kyoto University during the course of this work. M. T. and Y. H. are financially supported by the Japan Society for the Promotion of Science.

## References

- Alves, J., & Homeier, N. 2003, *ApJL*, 589, L45  
 Blum, R. D., Schaerer, D., Pasquali, A., Heydari-Malayeri, M., Conti, P. S., & Schmutz, W. 2001, *AJ*, 122, 1875  
 Burch, D., Richartd, P., Blake, R. L. 1971, *Phys. Rev. Lett.*, 26, 1355  
 Conti, P. S., & Blum, R. D. 2002, *ApJ*, 564, 827  
 Campbell, B., et al. 1992, *AJ*, 104, 1721  
 Cantó, J., Raga, A. C., & Rodríguez, L. F. 2000, *ApJ*, 536, 896  
 Clark, J. S., Negueruela, I., Crowther, P. A., & Goodwin, S. P. 2005, *A&A*, 434, 949  
 Cotera, A. S., Erickson, E. F., Colgan, S. W. J., Simpson, J. P., Allen, D. A., & Burton, M. G. 1996, *ApJ*, 461, 750  
 Däppen, W. 2000, in *Allen's Astrophysical Quantities*, ed. A. N. Cox (New York: Springer-Verlag), 27  
 Figer, D. F., Kim, S. S., Morris, M., Serabyn, E., Rich, R. M., & McLean, I. S. 1999, *ApJ*, 525, 750  
 Figer, D. F., et al. 2002, *ApJ*, 581, 258  
 Figer, D. F. 2005, *Nature*, 434, 192  
 Garmire, G. P., Bautz, M. W., Ford, P. G., Nousek, J. A., & Ricker, G. R. 2003, *Proc. SPIE*, 4851, 28  
 Gullikson, E. M. 2001, in *X-ray Data Booklet*, ed. A. Thompson et al. (Berkeley: University of California), 1-38  
 House, L. L. 1969, *ApJS*, 18, 21  
 Kokubun, M., et al. 2006, *PASJ*, submitted  
 Kortright, J. B. 2001, in *X-ray Data Booklet*, ed. A. Thompson et al. (Berkeley: University of California), 1-28  
 Koyama, K., Maeda, Y., Sonobe, T., Takeshima, T., Tanaka, Y., & Yamauchi, S. 1996, *PASJ*, 48, 249  
 Koyama, K., et al. 2006, *PASJ*, in press.  
 Koyama, K., et al. 2006, *PASJ*, submitted.  
 Koyama, K., et al. 2006, *PASJ*, submitted.  
 Lang, C. C., Goss, W. M., & Morris, M. 2001, *AJ*, 121, 2681  
 Lang, C. C., Johnson, K. E., Goss, W. M., & Rodríguez, L. F. 2005, *AJ*, 130, 2185  
 Law, C., & Yusef-Zadeh, F. 2004, *ApJ*, 611, 858  
 Liedahl, D. A. 1998, in *Lecture Notes in Physics* vol. 520, ed. J. van Paradijs, & J. A. M. Bleeker (Berlin: Springer-Verlag), 189  
 Mitsuda, K., et al. 2006, *PASJ*, submitted.  
 Moffat, A. F. J. 1983, *A&A*, 124, 273  
 Morris, M., & Serabyn, E. 1996, *ARA&A*, 34, 645  
 Murakami, H., Koyama, K., Sakano, M., Tsujimoto, M., & Maeda, Y. 2000, *ApJ*, 534, 283  
 Nagata, T., Woodward, C. E., Shure, M., & Kobayashi, N. 1995, *AJ*, 109, 1676  
 Najarro, F., Figer, D. F., Hillier, D. J., & Kudritzki, R. P. 2004, *ApJL*, 611, L105  
 Paerels, F. 1998, in *Lecture Notes in Physics* vol. 520, ed. J. van Paradijs, & J. A. M. Bleeker (Berlin: Springer-Verlag), 347  
 Park, S., Munro, M. P., Baganoff, F. K., Maeda, Y., Morris, M., Howard, C., Bautz, M. W., & Garmire, G. P. 2004, *ApJ*, 603, 548  
 Predehl, P., Costantini, E., Hasinger, G., & Tanaka, Y. 2003, *Astronomische Nachrichten*, 324, 73  
 Raga, A. C., Velázquez, P. F., Cantó, J., Masciadri, E., & Rodríguez, L. F. 2001, *ApJL*, 559, L33  
 Revnivtsev, M. G., et al. 2004, *A&A*, 425, L49  
 Reynolds, C. S., & Nowak, M. A. 2003, *Phys. Rep.*, 377, 389  
 Rockefeller, G., Fryer, C. L., Melia, F., & Wang, Q. D. 2005, *ApJ*, 623, 171  
 Rodríguez-Fernández, N. J., Martín-Pintado, J., & de Vicente, P. 2001, *A&A*, 377, 631  
 Serabyn, E., Shupe, D., & Figer, D. F. 1998, *Nature*, 394, 448  
 Serlemitsos, P., et al. 2006, *PASJ*, submitted.  
 Shibata et al. 2001, *Applied Optics*, 40, 22, 3762  
 Silich, S., Tenorio-Tagle, G., & Rodríguez-González, A. 2004, *ApJ*, 610, 226  
 Smith, R. K., Brickhouse, N. S., Liedahl, D. A., & Raymond, J. C. 2001, *ApJL*, 556, L91  
 Sofia, U. J., Cardelli, J. A., & Savage, B. D. 1994, *ApJ*, 430, 650  
 Stolte, A., Grebel, E. K., Brandner, W., & Figer, D. F. 2002, *A&A*, 394, 459  
 Sunyaev, R. A., Markevitch, M., & Pavlinsky, M. 1993, *ApJ*, 407, 606  
 Takahashi, T., et al. 2006, *PASJ*, submitted  
 Tatischeff, V. 2002, *astro-ph/0208397*  
 Tsujimoto, M., Feigelson, E. D., Grosso, N., Micela, G., Tsuboi, Y., Favata, F., Shang, H., & Kastner, J. H. 2005, *ApJS*, 160, 503  
 Uchiyama, Y., Takahashi, T., & Aharonian, F. A. 2002, *PASJ*, 54, L73  
 Valinia, A., Tatischeff, V., Arnaud, K., Ebisawa, K., & Ramaty, R. 2000, *ApJ*, 543, 733  
 Wang, Q. D., Dong, H., & Lang, C. 2006, *MNRAS*, 371, 38  
 Weisskopf, M. C., Brinkman, B., Canizares, C., Garmire, G., Murray, S., & Van Speybroeck, L. P. 2002, *PASP*, 114, 1  
 Yang, Y., Park, H. S., Lee, M. G., & Lee, S.-G. 2002, *Journal of Korean Astronomical Society*, 35, 131  
 Yusef-Zadeh, F., Law, C., Wardle, M., Wang, Q. D., Fruscione, A., Lang, C. C., & Cotera, A. 2002, *ApJ*, 570, 665  
 Yusef-Zadeh, F., Law, C., & Wardle, M. 2002, *ApJL*, 568, L121